Available online at www.sciencedirect.com
ScienceDirect
Journal of the European Ceramic Society 29 (2009) 2105–2118
www.elsevier.com/locate/jeurceramsoc

Oxidation behaviour of a (Mo, W)Si_2-based composite in dry and wet oxygen atmospheres in the temperature range 350–950 °C

K. Hellström [a,*], J.E. Tang [b], T. Jonsson [b], M. Halvarsson [b], R. Pompe [c], M. Sundberg [d], J.-E. Svensson [a]

[a] *Department of Chemical and Biological Engineering, Chalmers University of Technology, Kemivägen 10, SE-412 96 Göteborg, Sweden*
[b] *Department of Applied Physics, Chalmers University of Technology, SE-412 96 Göteborg, Sweden*
[c] *IVF/Swedish Ceramic Institute, Argongatan 30, SE-43153 Mölndal, Sweden*
[d] *Kanthal AB, 734 27 Hallstahammar, Sweden*

Received 16 September 2008; received in revised form 26 November 2008; accepted 4 December 2008
Available online 22 January 2009

Abstract

The oxidation of a (Mo, W)Si_2-based composite was investigated in the temperature range (350–950 °C). The influence of temperature and water vapour on the oxidation was examined. The kinetics was studied using a thermobalance whereas the morphology and composition of the oxides were examined using X-ray diffractometer (XRD), scanning electron microscope (SEM), transmission electron microscope (TEM) and energy dispersive X-ray (EDX). Focused ion beam (FIB) milling was performed on some of the oxide scales which allowed us to look at a non-mechanically disturbed scale/oxide in cross-section. Rapid oxidation was found to occur in the 550–750 °C temperature range. The mass gains were significantly larger in O_2 than in $O_2 + 10\%H_2O$. The different mass changes in the two exposure atmospheres were attributed to the higher vapour pressure of the volatile $MoO_2(OH)_2$ and $WO_2(OH)_2$ species in $O_2 + 10\%H_2O$ than that of $(MoO_3)_3$ and $(WO_3)_3$ in dry O_2. The peak mass gain was found to occur at a temperature of about 750 °C in O_2 and 650 °C in $O_2 + 10\%H_2O$. At temperatures above 850 °C, especially when water vapour is present, the removal of Mo and W from the oxide scales is rapid enough to allow partial healing of the silica, causing the oxidation rate to drop. At 950 °C in $O_2 + 10\%H_2O$, a protective SiO_2 scale could be re-established quickly and maintained, causing the oxidation to essentially cease.

Keywords: (Mo, W)Si_2; Corrosion; Silicides; SiO_2; Refractories

1. Introduction

(Mo, W)Si_2-based composites are used as heating elements in industrial furnaces that can be operated at temperatures up to 1850 °C. The material has good oxidation resistance at high temperatures, i.e. above 900 °C, which is due to the formation of a protective self-healing silica scale. At lower temperatures the material suffers from accelerated oxidation due to the formation of a non-protective oxide scale.

The oxidation reactions of (Mo, W)Si_2 in the temperature region where accelerated oxidation takes place is described in reaction (1).[1] Simultaneous oxidation of W, Mo and Si takes place.

$$2\text{Mo(or W)}Si_2 + 7O_2 \rightarrow 2\text{Mo(or W)}O_3 + 4SiO_2 \quad (1)$$

At higher temperatures where a protective SiO_2 scale can be established the oxidation reaction is described in reaction (2). Selective oxidation of Si takes place.

$$10\text{Mo(or W)}Si_2 + 16O_2 \rightarrow 2\text{Mo(or W)}_5Si_3 + 6SiO_2 \quad (2)$$

In an environment with very low oxygen pressure only Si can be oxidised as given in reactions (3) and (4).[2]

$$\text{(Mo, W)}Si_2(s) + 2O_2(g) \rightarrow \text{Mo, W(s)} + 2SiO_2(s) \quad (3)$$

$$\text{(Mo, W)}_5Si_3(s) + 3O_2(g) \rightarrow \text{Mo, W(s)} + 3SiO_2(s) \quad (4)$$

It was reported, from differential thermal analysis (DTA) studies in air, that oxidation of WSi_2 powder starts at 500 °C and is completed above 1100 °C.[3] An exothermal peak at 910 °C

* Corresponding author. Tel.: +46 31 7722859; fax: +46 31 7722853.
E-mail address: krh@chalmers.se (K. Hellström).

0955-2219/$ – see front matter © 2008 Elsevier Ltd. All rights reserved.
doi:10.1016/j.jeurceramsoc.2008.12.009

was reported to correspond to WO_3 formation and another exothermal peak at 825 °C to the formation of $WO_{2.75}$. This was suggested to be due to interaction of WSi_2 with WO_3. A DTA study was also performed on $MoSi_2$. It was reported that an exothermic peak at 485 °C corresponded to the formation of MoO_3 and an endothermic peak at 790 °C to its evaporation.

The aim of this investigation is to understand the mechanism of the oxidation behaviour of a (Mo, W)Si_2-based composite in the temperature range 350–950 °C in dry and wet O_2 atmospheres. In order to examine the oxidation mechanisms, the oxidation rates were tracked using thermogravimetric analysis and the oxide scales were investigated using a combination of analysis techniques such as X-ray diffraction and electron microscopy.

2. Experimental

In this investigation, a commercial clay-bonded (Mo, W)Si_2-based composite manufactured by Kanthal AB of Sweden under the product name Kanthal Super 1900 (KS 1900) was studied. This material is used in heating elements in high temperature furnaces and is manufactured by mixing (Mo, W)Si_2 powder, clay (bonding material) and water. The major components of the clay are SiO_2 and Al_2O_3. The mixture is extruded into 3-mm diameter rods, dried and then sintered at high temperatures. During the final step, a SiO_2 scale is formed on the surface of the material. After sintering the material is more than 99% dense. It consists of a major (Mo, W)Si_2 phase with about 10% of (Mo, W)$_5Si_3$ and 10% of bonding material (clay). The material was supplied in the form of 10 cm-long rods.

The rods were cut into 2.0–3.5 cm-long sections using a high-speed diamond saw. The cross-section surfaces were polished with 320-grit SiC paper. A 1.15-mm through-hole was drilled near one end of each specimen for thermogravimetric analysis (TGA). Before exposure the specimens were cleaned ultrasonically, first with distilled water followed by ethanol and finally with acetone. The samples were then dried in flowing air and their weight was recorded before and after exposure.

The exposures were performed in a SETARAM TGA system with a 14-mm diameter SiO_2-glass tube in the furnace. The isothermal exposures were carried out at various temperatures ranging from 350 °C to 950 °C in a furnace system that was fitted with a humidifier, which produced a flowing reaction gas consisting of dry O_2 ($H_2O < 5$ ppm) or $O_2 + 10\%H_2O$ (=0.9 at $O_2 + 0.1$ at. H_2O). 20 ml/min was passed through the furnace system.

Before investigating the cross-section of the oxide scale, the samples were embedded in a resin and polished using increasingly finer grades of diamond suspension, finishing at 1 μm. The sample surfaces were then carbon coated.

The microstructure of the cross-section oxide scales was examined with a Camscan S4-80DV scanning electron microscope (SEM) using the backscattered electron imaging mode. The SEM was equipped with a Link eXL energy dispersive X-ray (EDX) spectroscopy system. An accelerating voltage of 8 kV was used for SEM imaging and 20 kV for the SEM/EDX analyses. The morphology of the oxide scales was examined with an ElectroScan 2020 environmental scanning electron microscope (ESEM) in the secondary electron mode. The ESEM was equipped with a Link Isis EDX system. An accelerating voltage of 20 kV was used. Additionally, a Philips CM 200 transmission electron microscope (TEM) was used to investigate the composition of the oxide scale. The TEM was equipped with a Link Isis EDX system and an accelerating voltage of 200 kV was used.

Focused ion beam (FIB) milling was performed on selected sites on the curved surface of the oxidised rods. At each site, a chunk of material (up to 80 μm × 100 μm × 60 μm) was sputtered away to reveal a cross-section of the oxide scale and the bulk material beneath it. The aim of this operation was to complement the cross-section SEM analyses performed on epoxy resin-cast samples with analyses performed on oxidised samples that have undergone no sample preparation and thus are less affected by mechanical grinding and polishing. This method offers a convenient way to image the undisturbed oxide scale morphology at any site of interest both in top view and in cross-section view, thereby allowing a better understanding of the structure of various oxide features. The milling was performed in a FEI FIB200THP workstation and a FEI DualBeam Strata 235 FIB/SEM workstation, both running on a liquid gallium ion source at 30 kV. A beam current setting of 20 nA was selected for initial coarse milling and was progressively switched to lower beam currents (finishing at 50 pA) to achieve a smooth surface and to minimise re-deposition.

The FIB-milled cross-sections were also analysed using a LEO 1550 Gemini SEM operated at 20 kV. The main investigative methods employed were backscattered electron imaging and EDX analysis using a Link Isis system.

Analyses of the crystalline composition of the oxide scales were performed using a Siemens D5000 X-ray diffractometer (XRD) with grazing-incidence set up. Incidence angles of 1–10° were used depending on the oxide scale thickness.

3. Results and discussion

3.1. Kinetics

The (Mo, W)Si_2-based composite showed similar trends of mass gain as a function of time when oxidised isothermally at various temperatures in the range 350–950 °C in either the O_2 or $O_2 + 10\%H_2O$ atmosphere (Figs. 1 and 2) although the mass gains are significantly larger in dry O_2.

The mass gain increases with exposure temperature up to 650 °C in $O_2 + 10\%H_2O$ and up to 650 °C or 750 °C in O_2. Spallation due to a very loosely adherent oxide scale is noted in the mass change vs. exposure time curves. At 750 °C in O_2 the spallation of the oxide is most severe. This is probably due to a more rapidly growing oxide scale. Thus, the peak oxidation temperature in O_2 is likely to be around 750 °C although the mass gain could not be determined due to severe spallation.

The mass gain up to 650–750 °C is probably due to the normal increase of the reaction rate with temperature. At higher temperatures the mass gain starts dropping off. This may be explained as a combined effect of evaporation from

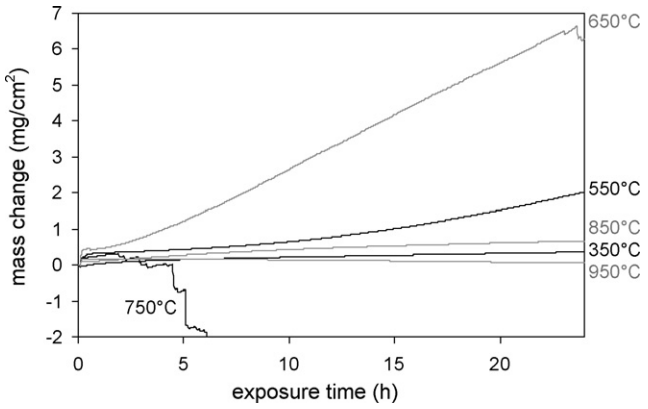

Fig. 1. (Mo, W)Si_2 composite exposed in a thermobalance in O_2 for 24 h at different temperatures.

the samples and the formation of a more protective scale. At 850 °C the mass gain is slow in O_2, in $O_2 + 10\%H_2O$ there is first a mass gain and thereafter a significant mass loss. The mass loss represents either spallation or evaporation from the samples, with evaporation being the most likely event, since no signs of spallation were observed. At 950 °C in O_2 there is first an increase in mass and thereafter a decrease, indicating evaporation from the sample. At this temperature the formation and evaporation of MoO_3 is likely to occur more or less simultaneously. Hence, the increase in mass may be due to formation of WO_3, whereas the decrease is likely to be due to its evaporation. At 950 °C in $O_2 + 10\%H_2O$ there is a slight initial mass gain. However, the curve quickly levels off and remains flat for the remaining duration of the exposure. It is believed that, owing to the rapid and effective removal of MoO_3 and WO_3 from the oxide scale, a dense and protective silica scale is formed and maintained, which protects the material from further oxidation.

Fig. 3 shows the mass change of the samples exposed in $O_2 + 10\%H_2O$ and O_2, respectively, after 24 h exposure as a function of exposure temperature. This was made easier to be able to link the mass change to the oxide thickness, as will be discussed later.

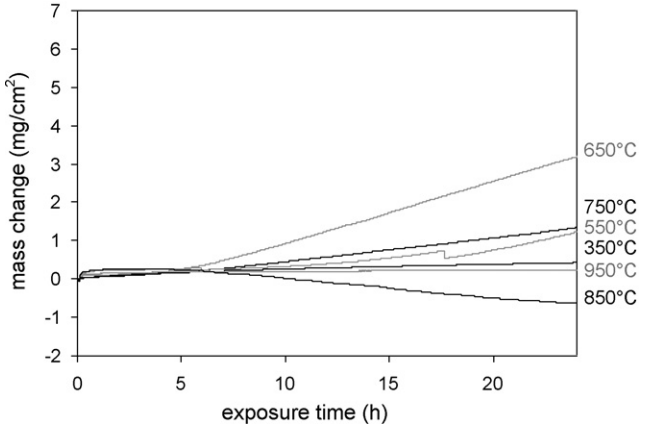

Fig. 2. (Mo, W)Si_2 composite exposed in a thermobalance in $O_2 + 10\%H_2O$ for 24 h at different temperatures.

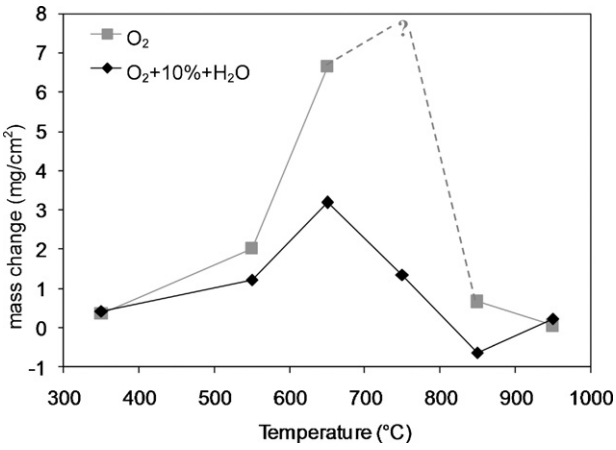

Fig. 3. Mass change vs. exposure temperature curve of (Mo, W)Si_2 composite samples exposed in O_2 or $O_2 + 10\%H_2O$ for 24 h.

3.2. X-ray diffraction (XRD)

Samples oxidised in dry O_2 for 24 h at 350–950 °C were analysed using XRD. The X-ray spectra together with peak positions of the $W_{0.5}Mo_{0.5}Si_2$, $W_3Mo_2Si_3$, MoO_3, WO_3 and $W_{0.71}Mo_{0.29}O_3$ are shown in Fig. 4. The X-ray spectra of the unexposed material and the samples oxidised at 350 °C and 450 °C are similar with peaks only from the base material, $W_{0.5}Mo_{0.5}Si_2$, and $W_3Mo_2Si_3$, indicating that the oxide scales are thin or amorphous. Samples oxidised at 550 °C exhibit peaks corresponding to MoO_3, WO_3 and/or (Mo, W)O_3. An amorphous SiO_2 is also most likely to form. The MoO_3 peaks have disappeared on the 650 °C specimen, indicating evaporation of any formed MoO_3. The mixed W–Mo-oxide peaks disappear and more specific WO_3 peaks appear with increasing exposure temperature, i.e. 750–950 °C. Samples exposed at 950 °C also exhibit peaks corresponding to cristobalite SiO_2, showing that crystallisation of the scale has taken place.

The XRD spectra of samples oxidised in $O_2 + 10\%H_2O$ for 24 h exhibit similar patterns to the unexposed material after exposure at 350 °C, 450 °C and 950 °C (Fig. 5), indicating that the oxide scales are very thin or amorphous. Moreover, the XRD patterns of the samples exposed at 950 °C exhibit peaks corresponding to $W_{0.5}Mo_{0.5}$, indicating a very protective scale with selective oxidation of Si through reactions (3) and/or (4). After exposure at 550–850 °C WO_3 and/or a mixed oxide of Mo and W is detected whereas no MoO_3 peaks are visible. The lack of MoO_3 peaks at 550 °C in $O_2 + 10\%H_2O$ indicates that any MoO_3 formed evaporates at a lower temperature in $O_2 + 10\%H_2O$ than in O_2. The lack of WO_3 peaks at 950 °C in $O_2 + 10\%H_2O$ indicates that WO_3 also evaporates at a lower temperature in $O_2 + 10\%H_2O$ than in dry O_2.

3.3. Evidence of Mo and W evaporation

During the (Mo, W)Si_2 composite oxidation tests, particles were deposited downstream, in the cooler parts of the exposure tube. Deposits were collected after exposure at 750 °C in both O_2 and $O_2 + 10\%H_2O$. EDX showed that the deposits consisted

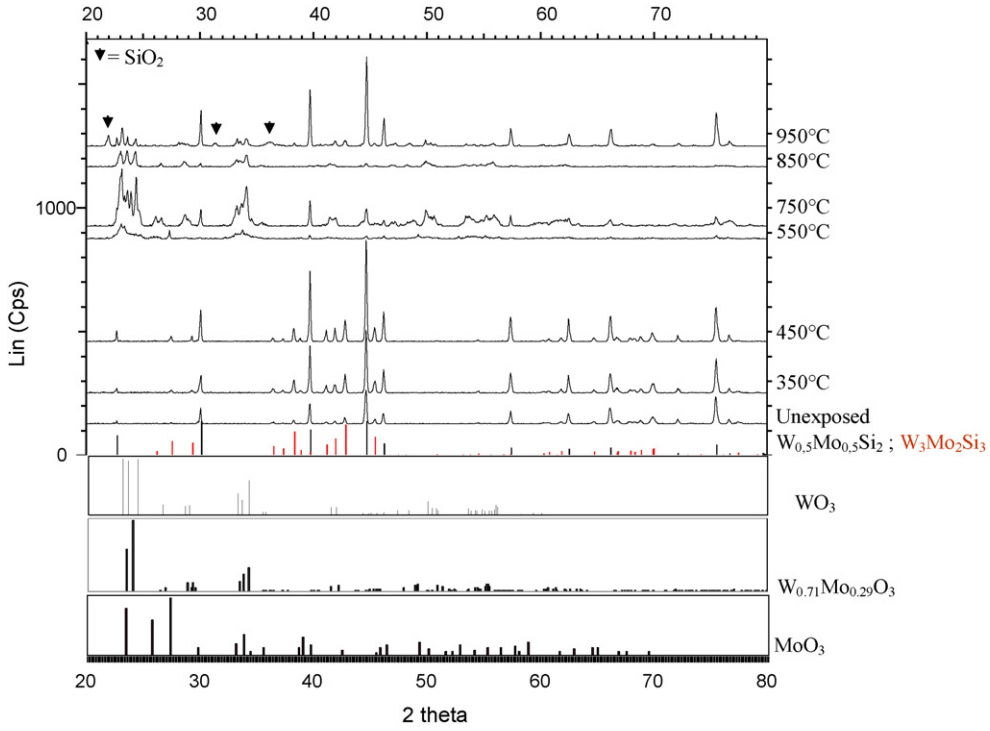

Fig. 4. XRD of (W, Mo)Si_2 samples exposed in a thermobalance for 24 h in O_2 at different temperatures.

of Mo and W but only MoO_3 could be detected by XRD. This indicates that both Mo- and W-bearing species evaporate but the evaporation of Mo-containing species predominates. This is in agreement with the XRD results, where WO_3 is detected in the oxide scale while MoO_3 is absent at 750 °C.

In the literature, it has been reported that the most abundant vapour species in equilibrium with MoO_3 powder at 850 °C are $(MoO_3)_3$, $(MoO_3)_4$, and $(MoO_3)_5$ with the ratio of about 20:7:1.[4] Therefore, it is reasonable to believe that the loss of MoO_3 in an O_2 atmosphere is mainly caused by the formation of volatile $(MoO_3)_3$, as described in reaction (5).

$$3MoO_3(s) \rightarrow (MoO_3)_3(g) \quad (5)$$

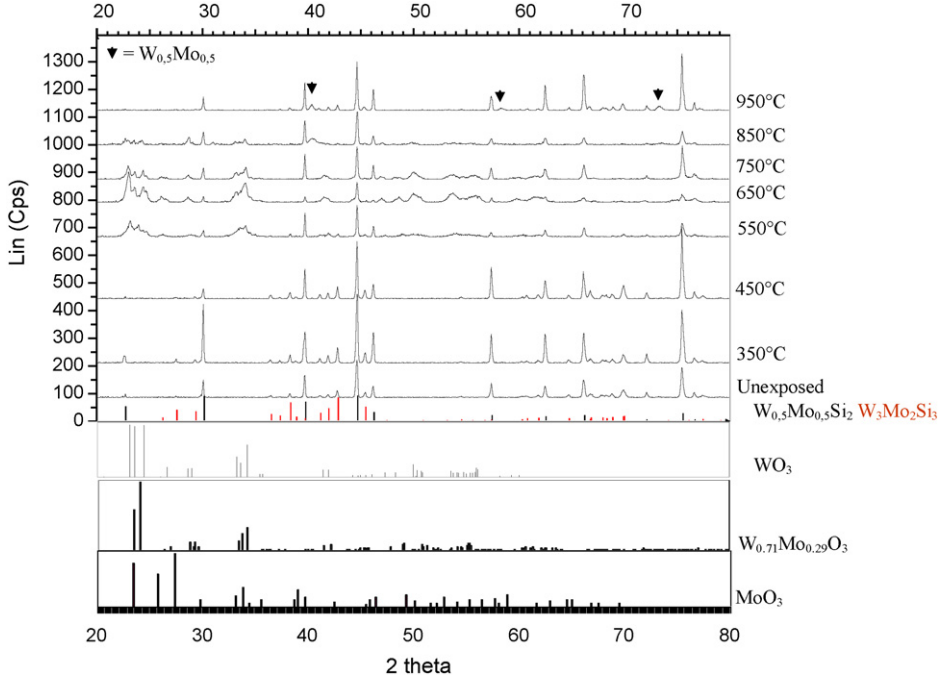

Fig. 5. XRD of (W, Mo)Si_2 samples exposed in a thermobalance for 24 h in O_2 + 10%H_2O at different temperatures.

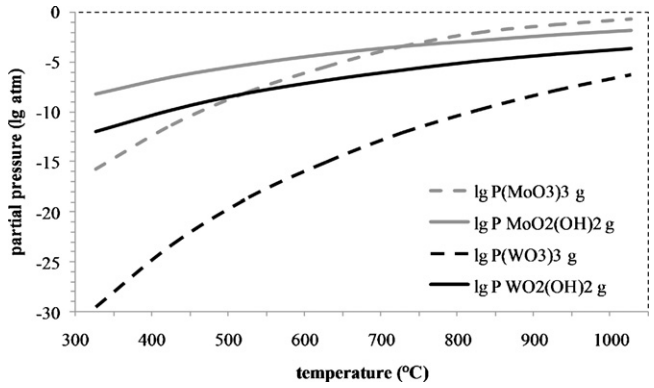

Fig. 6. The equilibrium partial pressures of the gaseous species $(MoO_3)_3$, $(WO)_3$ in dry O_2 and $MoO_2(OH)_2$ and $WO_2(OH)_2$ in $O_2 + 10\%H_2O$.

It has been proposed that the volatility of $(WO_3)_3$ is higher than that of WO_3, which was attributed to the higher coordination.[5] This is also in agreement with thermodynamical calculations of the vapour pressure (Fig. 6). Therefore, it is reasonable to believe that the loss of WO_3 in an O_2 atmosphere is mainly caused by the formation of volatile $(WO_3)_3$, as described in reaction (6).

$$3WO_3(s) \rightarrow (WO_3)_3(g) \quad (6)$$

Another study showed that water vapour increased the volatility of MoO_3 and WO_3 at 1000 °C,[6] presumably due to the formation of $MoO_2(OH)_2$ and $WO_2(OH)_2$, respectively,[5] which is in agreement with our previous study of MoO_3-containing oxide scales.[7] Therefore, it is reasonable to conclude that the loss of MoO_3 and WO_3 in an atmosphere of $O_2 + 10\%H_2O$ is also due to the formation of volatile $MoO_2(OH)_2$ and $WO_2(OH)_2$, respectively, as described in reactions (7) and (8).

$$MoO_3(s) + H_2O(g) \rightarrow MoO_2(OH)_2(g) \quad (7)$$

$$WO_3(s) + H_2O(g) \rightarrow WO_2(OH)_2(g) \quad (8)$$

The equilibrium partial pressures of $(MoO_3)_3$ and $(WO_3)_3$ in dry O_2 and of $MoO_2(OH)_2$ and $WO_2(OH)_2$ in $O_2 + 10\%H_2O$ were calculated (Fig. 6). The tabulated Gibbs energies of formation were used in the calculations.[8,9] It is clear that the equilibrium vapour pressure of $MoO_2(OH)_2$ in $O_2 + 10\%H_2O$ is higher than that of $(MoO_3)_3$ in dry O_2 below ~750 °C. This is consistent with the XRD results, in that MoO_3 is lost at a lower temperature from the samples that were oxidised in $O_2 + 10\%H_2O$ than in dry O_2. It is also clear from Fig. 6 that the vapour pressure of $WO_2(OH)_2$ in $O_2 + 10\%H_2O$ is substantially higher than that of $(WO_3)_3$ in dry O_2, indicating a faster evaporation rate of W-containing species from the oxide scales oxidised in $O_2 + 10\%H_2O$ than in O_2. This is consistent with the kinetic and XRD results. The mass gains of the samples oxidised in $O_2 + 10\%H_2O$ are much less than those measured on samples oxidised in dry O_2 (see Figs. 1–3). WO_3 were detected by XRD on samples exposed at 950 °C in O_2 but not in $O_2 + 10\%H_2O$ (see Figs. 4 and 5).

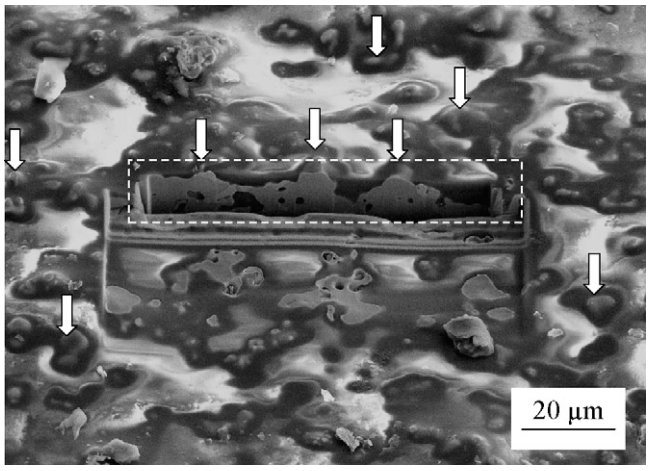

Fig. 7. SEM image of the top surface of an unexposed sample viewed at a 45° tilt angle. It is covered in silica glass and features a number of protruding "knolls" (arrowed). The dotted frame indicates FIB-milled cross-section.

3.4. The morphology and composition of the oxide scales

3.4.1. Morphology of as-received samples

A number of as-received sample rods were examined prior to the laboratory exposures in order to characterise the microstructure before the start of oxidation. As expected, the outer surface was covered by silica glass due to the final heat treatment during production. The surface was uneven and featured a large number of "knolls" (arrowed in Fig. 7). FIB milling was carried out in order to view these "knolls" in cross-section. As can be seen in Fig. 7, the "knolls" are bulk material protrusions under a thin layer of silica glass. The composition of the silica scale was analysed with EDX; half of the analysed spots showed pure SiO_2. The other half had additions of about 1 at.% Ca, 1 at.% Al, 0.2 at.% Mg and 0.2 at.% Na, these might originate from the clay.

The bulk material is a composite that consists of a number of phases. This is evident from the atomic number contrast in the backscattered electron SEM image of the material cross-section in Fig. 8. The various regions were labelled according to grey level ("dark", "grey" and "white") and probed for their respective chemical compositions. The most dominant phase—the "grey" phase, contained 67 at.% Si along with 22–23 at.% Mo and 10–11 at.% W, making it the (Mo, W)Si_2 phase where the Mo:W ratio is approximately 2. In the well-defined "white" regions, the Si concentration stayed close to the average of 37 at.%. They were hence characterised as the (Mo, W)$_5Si_3$ phase. Unlike the (Mo, W)Si_2 phase where there was consistently around twice as much Mo as there was W, this phase contained significantly more W than Mo. The Mo:W ratio generally ranged from 0.3 to 0.7 although there was the occasional incidence of almost pure W_5Si_3. The "white" regions accounted for slightly under 10% of the analysed cross-section surface area. The "dark" regions were thought to have resulted from the use of bonding clay in the production. These regions contained about 90% SiO_2, 5% Al_2O_3, 3 at.% Mg, 1 at.% Ca, 0.5 at.% K and 0.5 at.% Na and these regions accounted for a little over 10% of the analysed cross-section surface area.

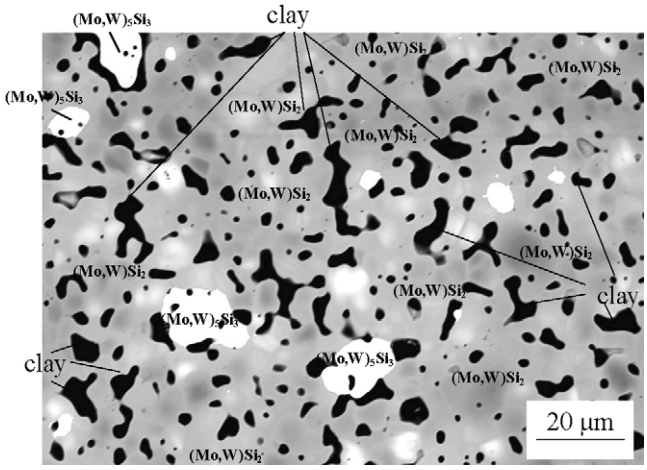

Fig. 8. SEM backscattered electron image of the bulk material in an un-exposed sample viewed in cross-section. The dominant "grey" type is (Mo, W)Si_2, the "white" is (Mo, W)$_5Si_3$ and the "dark" is the bonding clay consisting mostly of SiO_2.

3.4.2. The oxide growth at different temperatures in reference to the recorded mass gain: an overview of the trend

The mass gains after 24 h recorded for sample rods exposed to O_2 vs. $O_2 + 10\%H_2O$ atmosphere at temperatures ranging from 350 °C to 950 °C were shown in the mass gain vs. temperature plot in Fig. 3. It was observed that high mass gain generally corresponded to a thick oxide scale although the measured values were also affected by evaporation of species from the formed oxide.

A series of SEM images (see Figs. 9–12) taken of the surface oxide scale cross-section and surface morphology formed after 24 h at different temperatures in O_2 and $O_2 + 10\%H_2O$ gives an indication of the trend of measured mass gain vs. oxidation temperature (refer to Fig. 3).

The samples oxidised in dry and wet atmosphere at 350 °C showed little change in surface morphology and cross-sectioned microstructure from that of the unoxidised sample.

On the surface and the cross-section of the 450 °C samples, small oxide "sprouts" were found at a small number of sites but the amount was too small to be detected by XRD.

Interesting oxide formations covered the material surface on the 550 °C specimens. MoO_3 containing needles that were observed on the sample oxidised in O_2 atmosphere were absent from the sample oxidised in $O_2 + 10\%H_2O$, which also is consistent with the XRD results. Evaporation of $MoO_2(OH)_2$ through reaction (5) is a probable explanation.

The oxide scales formed at 650 °C and 750 °C in O_2 were, unfortunately, so delicate and adhered so poorly to the rods that even the slightest handling caused most of them to detach and collapse in a heap of fine powder. It was therefore impossible to obtain an image of their oxide scale morphologies and the cross-sections show only the oxide that is still attached to the rod after handling. An image of the whole cross-sectioned rod, slightly tilted, shows that the material is pesting at 750 °C (Fig. 11). Unlike the scales formed in dry O_2, the ones formed in $O_2 + 10\%H_2O$ yielded oxide scales that remained relatively intact, allowing their morphologies and microstructures to be imaged. The key difference is the apparently more compact structure of the oxide scale, which is probably due to the more effective removal of Mo- and W-containing species from it. Another contributing cause might be a change in viscosity of the SiO_2 scale by water adsorption,[10] however this is believed to have less importance since an earlier study showed that the healing of the silica scale on $MoSi_2$ can take place at 700 °C in O_2 atmosphere.[11] The higher temperature and thus diffusion speed makes the agglomeration of the Mo- and W-oxides clearly visible in the form of the small white dots in the oxide scales formed in both atmospheres at these temperatures.

Less oxide formed at 850 °C and 950 °C in both atmospheres; active evaporation of species from the oxide scale at higher temperatures caused the measured mass gains to be low. The oxides on the 950 °C specimens are more compact compared to the ones found after exposure at lower temperatures. A large number of WO_3-oxides are present in and on the SiO_2 scale formed during exposure in dry O_2, whereas no such oxides are present after exposure in wet atmosphere which is consistent with the XRD results. It appears that the oxide growth was effectively arrested during the 950 °C exposure in $O_2 + 10\%H_2O$. The surface morphology and cross-sectioned microstructure, while slightly different, bears a resemblance to that of the unoxidised specimen.

EDX results indicate more loss of Mo from the scale with increasing exposure temperature in O_2. The W/Mo ratio of the agglomerates was about 0.5 for the 550 °C specimens; 0.4–1.1 for 650 °C; 3.0–3.4 for 750 °C; 5.6–12 or pure W for 850 °C and only pure W for 950 °C. This is consistent with the XRD results where the mixed Mo-, W-oxide is gone at 950 °C and only WO_3 is detected. The same consistent pattern could not be found for the samples exposed in $O_2 + 10\%H_2O$. The cause is most likely that the Mo- and W-oxide removal rate is more similar in the presence of water vapour than in dry O_2 atmosphere.

It was of interest to take a closer look at the features on the oxide scale in order to understand processes involved in their formation. The samples exposed at 450 °C, 550 °C and 950 °C were subjected to detailed microanalysis. The 450 °C samples were selected as they were believed to be on the threshold of the beginning of oxidation. The 550 °C samples featured substantial oxide scales and interesting oxide geometries; they were believed to be at a fairly early stage of rapid oxidation. The 950 °C samples formed relatively thin oxides, indicating a major decrease in oxidation rate compared to the peak oxidation temperatures of 650–750 °C, which made interesting subjects for detailed microanalysis. The observations are presented below.

3.4.3. Detailed microanalysis on the oxide scale: the 450 °C exposures

In this section, the microstructure and the composition of the oxide scales formed during exposures at 450 °C in O_2 and $O_2 + 10\%H_2O$ are analysed in greater detail and compared. Fig. 13 shows the oxide scales of the two samples imaged at a tilt angle of about 45° in the SEM in backscattered electron

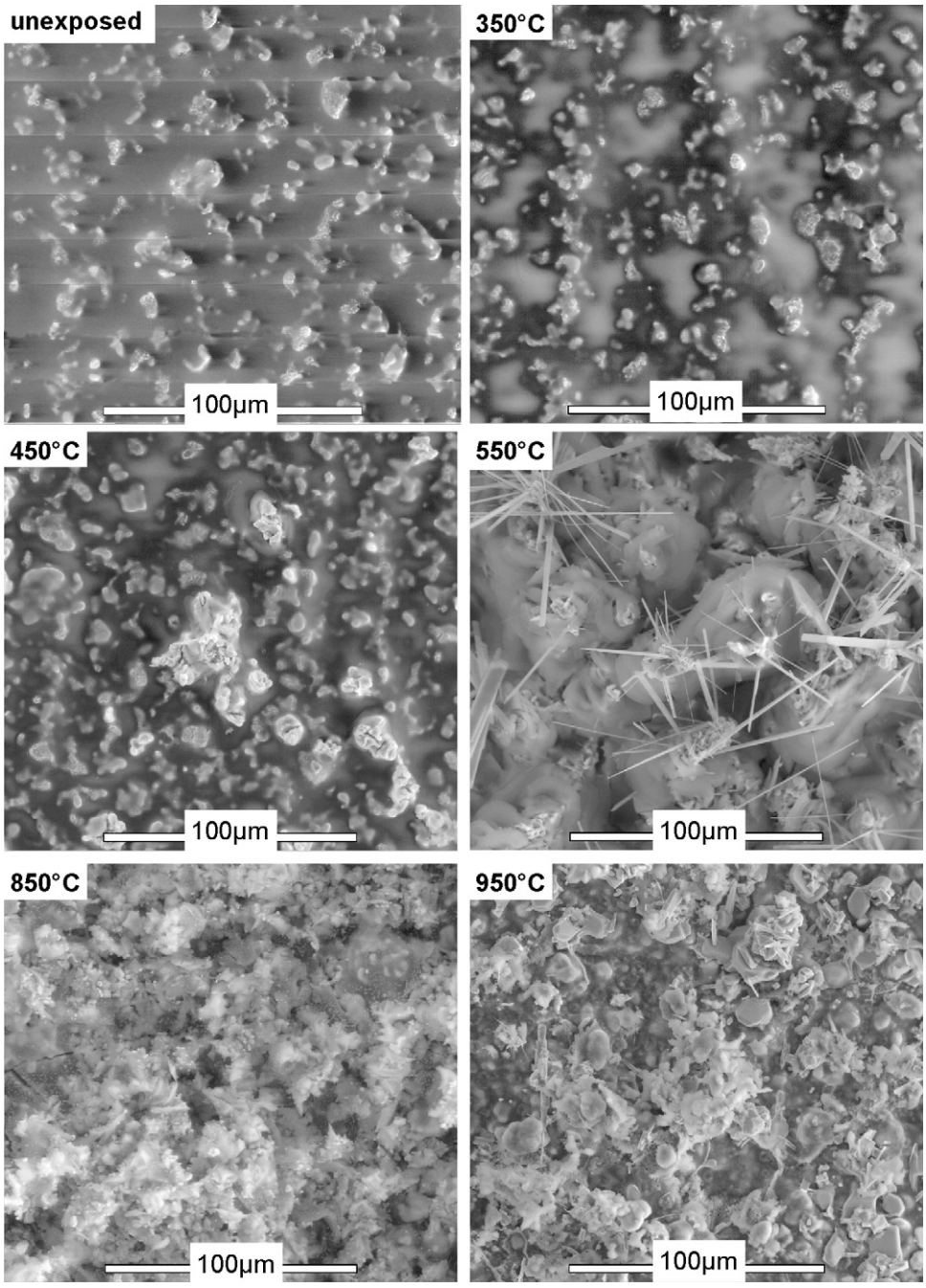

Fig. 9. ESEM images of (Mo, W)Si_2 samples exposed in a thermobalance for 24 h in O_2 at. different temperatures.

imaging mode. These images also show the FIB-milled sites revealing the cross-section for the purpose of investigating the interface between the oxide scale and the bulk material. It can be seen in these images that the sample surfaces are similar to that of an unexposed sample (compare with Fig. 7), covered in silica glass (from production heat-treatment) and featuring a number of "knolls".

The main difference is the emergence of "sprouts" (indicated in Fig. 13) that were found to be oxidised bulk material, i.e. Mo- and W-oxides embedded in SiO_2. The FIB-milled sites were planned so as to dissect some of these oxide "sprouts". The one in Fig. 13(b) was at an early stage and is seen to have grown out of the bulk material. It appears that these grew as a result of a local breakdown in protection offered by the silica glass, and hence the mostly likely nucleation sites would have been the "knolls" where the silica had been much thinner.

The EDX analysis also yielded an important observation: the Mo content of such oxide "sprouts" on the $O_2 + 10\%H_2O$ sample was systematically lower than on the O_2 sample. On average 16 at.% Mo (of the total cation content of the oxide; Si was at 73 at.% and W was at 11 at.%) was detected in the "sprouts" growing on the former while the corresponding value on the latter was 24 at.% (Si 66 at.%, W 11 at.%).

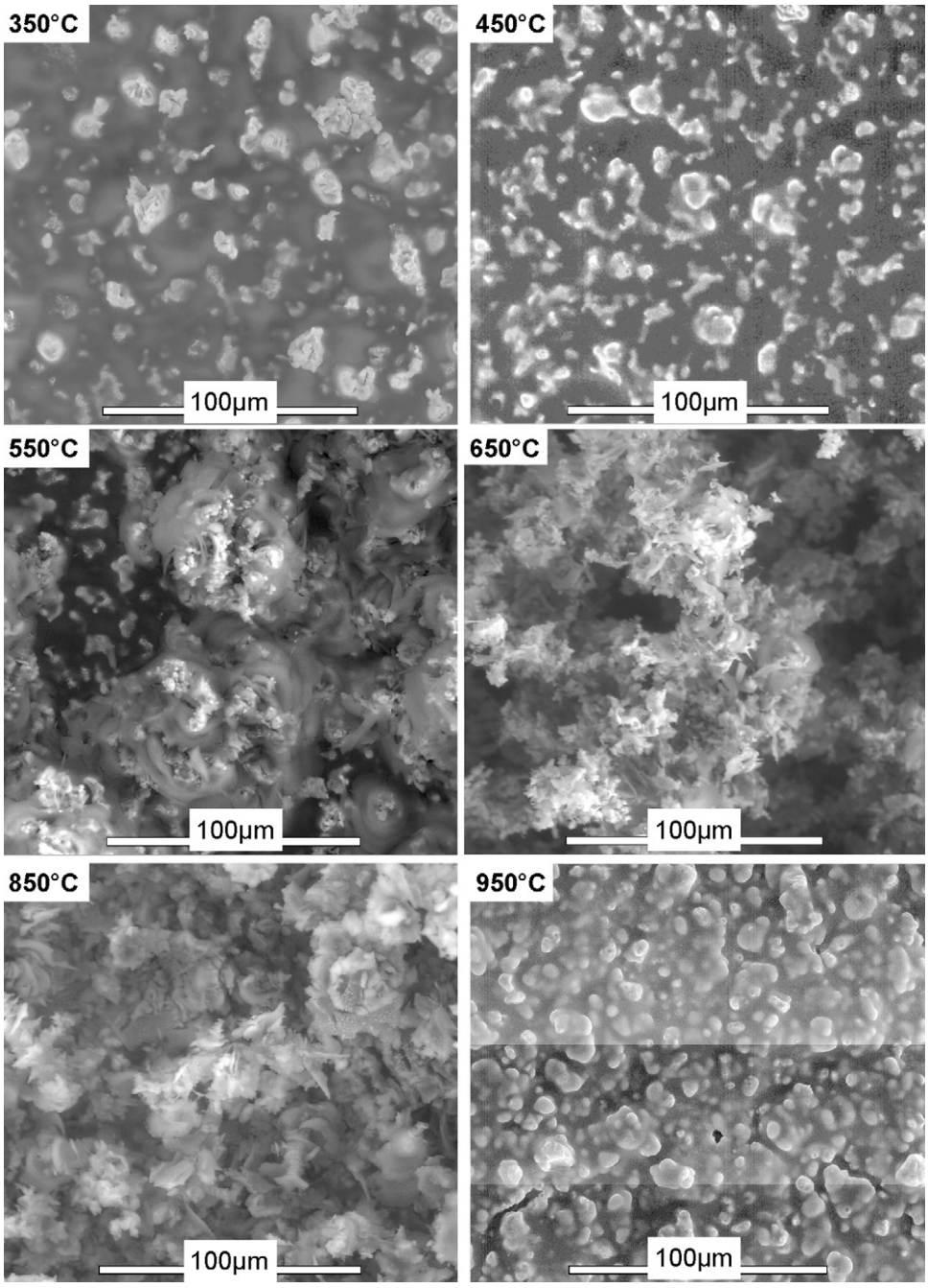

Fig. 10. ESEM images of (Mo, W)Si_2 samples exposed in a thermobalance for 24 h in O_2 + 10%H_2O at different temperatures.

3.4.4. Detailed microanalysis on the oxide scale: the 550 °C exposures

The 550 °C exposures resulted in the formation of delicate oxide features in the oxide scale. On the O_2 sample (see Figs. 14 and 9 (550 °C)), the morphology may be described as a rose-like, with bright needles protruding from the core. Through analysis of acquired element maps of the features (see Fig. 15), it was concluded that the needles were MoO_3. This observation is supported by the detection of this phase during XRD analysis (Fig. 4). The MoO_3-needles were most likely formed through re-deposition of evaporated $(MoO_3)_3$ from the scale.[7] WO_3 or a mixed Mo-, W-oxide was also detected during XRD analysis. Using EDX, most of the W was found to be concentrated in the bright oxide clumps in the core of the "roses", where a substantial amount of Mo was also found. The typical Mo and W contents (expressed as at.% of the cation content) were around 23 at.% and 13 at.%, respectively. The "petals" of the "roses" were also analysed and turned out to be mostly SiO_2, with no more than 3 at.% Mo and 5 at.% W.

Upon closer examination of these "roses", they appeared less like roses. These oxide "roses" featured "petals" that were more like disks. The "core", when viewed from an angle, resembled a slightly elongated hub built up by several tiers of disks. It is likely that the uneven surface (the "knolls") of the production samples

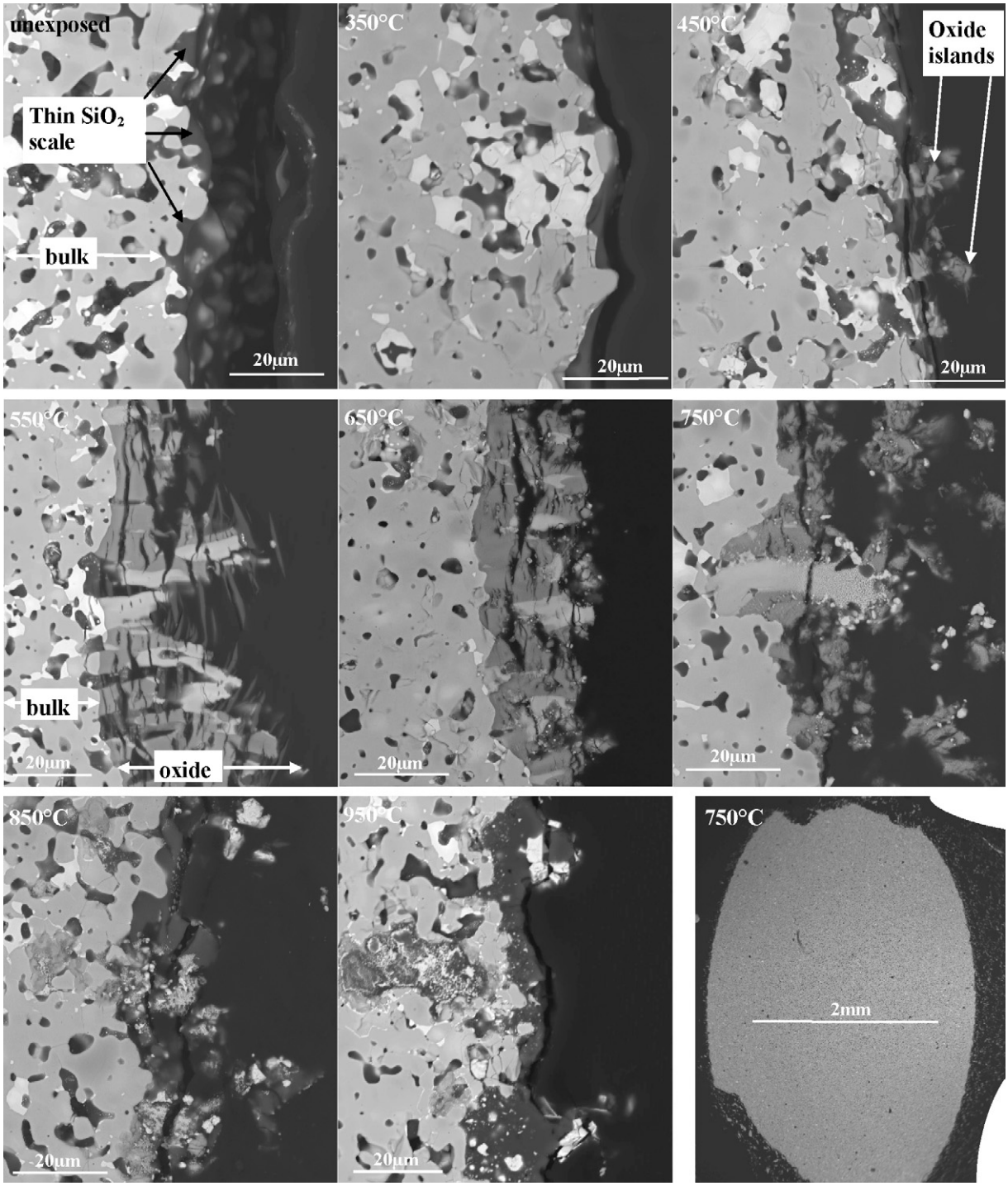

Fig. 11. Cross-section SEM images of an unexposed sample and samples exposed in dry O_2 at temperatures between 350 °C and 950 °C.

is the starting place for oxidation due to a thinner protective silica scale at these sites. As the oxidation front moves inwards oxidising the bulk material in the "knoll", the bulk material expands causing compressive stresses which results in horizontal cracks as the material is pushed outwards like rising columns. A FIB section at a site in the oxide scale is shown in Fig. 16, giving an idea of the structure.

Fig. 17 shows the cross-section of the oxide scale image in SEM backscattered mode. The oxidation front is indicated with markers. There are three distinct regions in the oxidised bulk material—a "dark" and a "bright" oxide region and a "very dark" region. The former was found to be an oxide scale with a Mo:W:Si composition similar to the (Mo, W)Si_2 phase in the bulk material. The latter was found to be one with Mo:W:Si compositions typical of the (Mo, W)$_5Si_3$ phase. It was concluded that they were, respectively, the oxidation products of the (Mo, W)Si_2 and the (Mo, W)$_5Si_3$ phases, consisting of MoO_3 and WO_3 in SiO_2. There was practically no variation in the "dark" oxidised

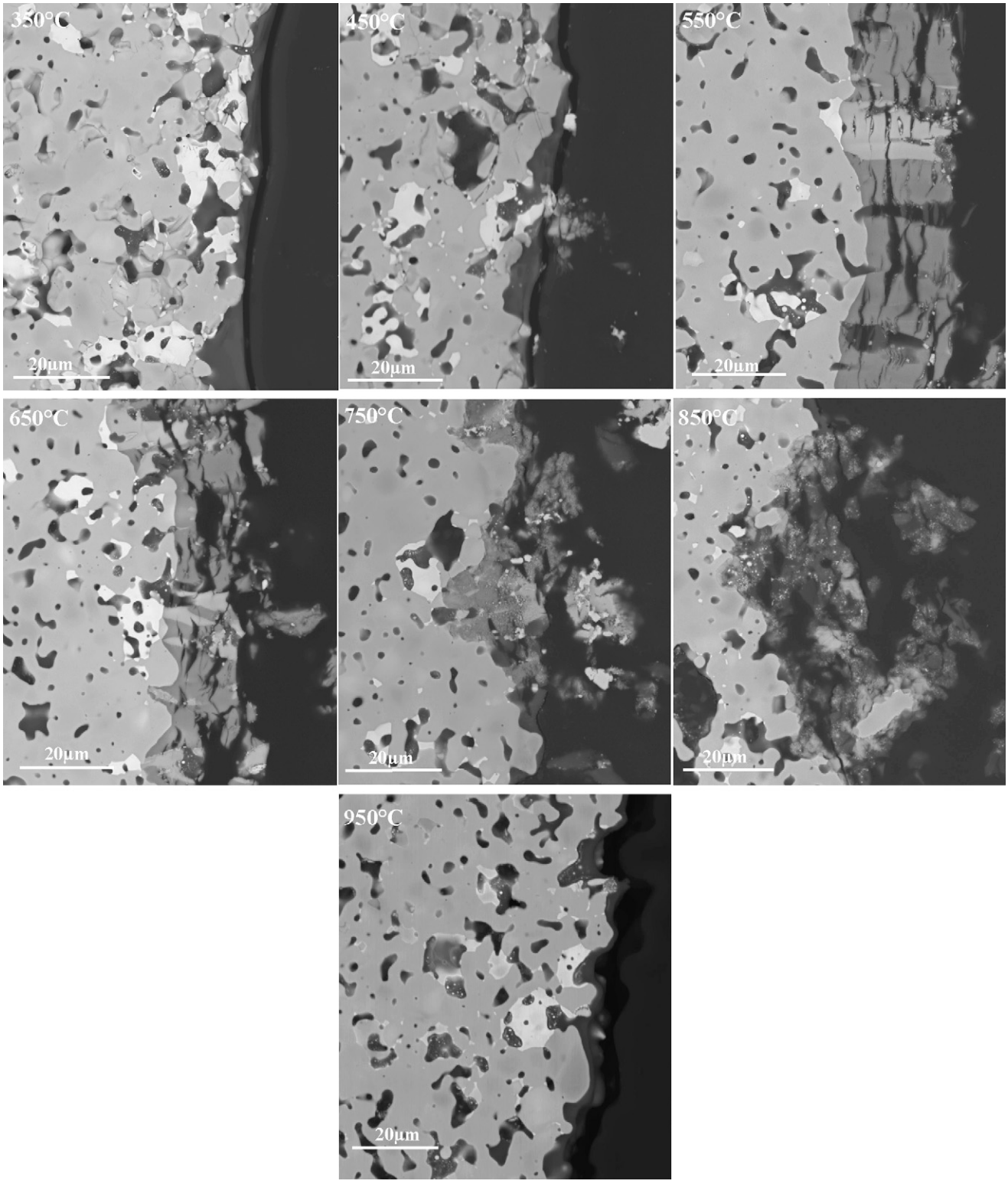

Fig. 12. Cross-section SEM images of samples exposed in O_2 + 10%H_2O at temperatures between 350 °C and 950 °C.

(Mo, W)Si_2 regions throughout the oxide scale. No variation was detected either in a single "bright" oxidised (Mo, W)$_5Si_3$ region but the Mo:W ratio could vary from one such region to another in view of the variation in the Mo:W ratio of the corresponding phase in the bulk material. The darker area in the oxide scale and in the bulk corresponds to the clay binder phase which consists of about 90% SiO_2, 5% Al_2O_3, 3 at.% Mg, 1 at.% Ca, 0.5 at.% K and 0.5 at.% Na. As the clay particles grow into the oxide scale they tend to elongate and crack due to tension produced by oxidation (volume-expanding (Mo, W)Si_2 and (Mo, W)$_5Si_3$ phases). The composition of the clay in the oxide scale is not changed—is the same as in the bulk. However, the clay introduces elements,

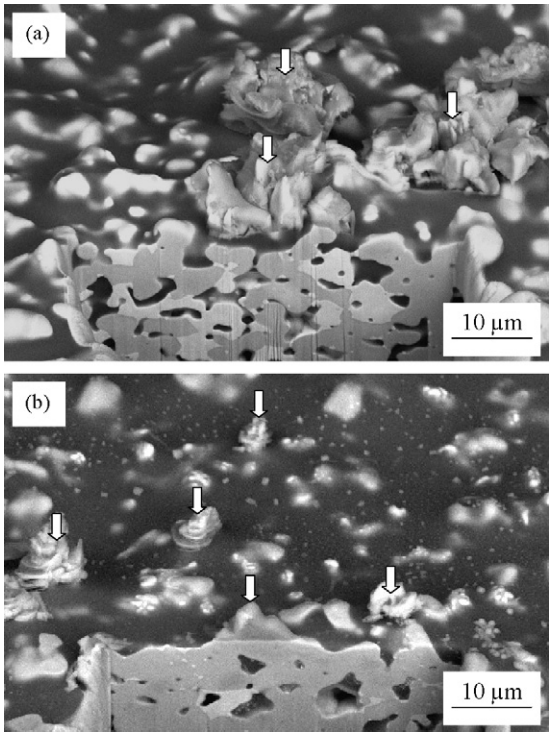

Fig. 13. SEM backscattered electron image of samples oxidised for 24 h at 450 °C in (a) O_2 atmosphere and (b) $O_2 + 10\%H_2O$ atmosphere. Cross-sections were milled using the FIB and the samples were viewed at a 45° tilt angle. The oxide "sprouts" are marked using arrows.

known to affect the viscosity of SiO_2,[10] to the oxide scale which might influence the oxidation rate. The elements mentioned would have different effects; Al as network-builder can be expected to potentially increase the viscosity whereas the network modifiers would decrease the viscosity. A decrease in viscosity would facilitate healing of defects in the oxide scale which would result in a lower oxidation rate. The diffusion rate of O_2 through the scale can of course also change when ions of different charge and size occupy interstitial sites. In general, the gas permeability decreases in silicate glasses as the concentration of modifier ions increases. However, since the major scale consists of modifier-free glass the oxidation rate is probably not affected.

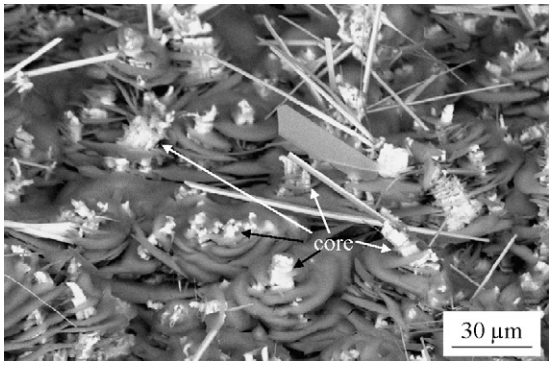

Fig. 14. SEM backscattered electron image of the oxide morphology on the surface of a sample oxidised for 24 h at 550 °C in O_2 atmosphere. The long bright needles are MoO_3. The "roses" are "petals" (consisting mostly of SiO_2) arranged in tiers around cores (oxidised bulk material, containing significant amounts of Mo and W).

On the oxide scale of the sample oxidised at 550 °C in $O_2 + 10\%H_2O$, a similar "rose" morphology was observed (see Figs. 18 and 10 (550 °C)). The MoO_3 needles were, however, absent, which was not surprising considering the effect of water vapour on the removal of Mo-oxide. Small bright particles peppered the cores of the "roses". The particles were too small for their compositions to be determined very accurately, but analyses indicated that they were likely to be oxides of Mo or W or combinations of both. No MoO_3 were confirmed with XRD. The oxides are then likely to be W-oxides or combinations of Mo- and W-oxides.

The oxide scale, when viewed in cross-section (see Figs. 12, 17 and 19), showed a marked difference from that on the sample oxidised in dry O_2. Mo- and W-rich bright particles could be seen and they were present in larger numbers in the outer regions of the oxide scale. Fig. 20 shows the outer oxide scale in cross-section view at higher magnification. It can be seen here that these bright particles are distributed at the rims of voids and crevices, and are invariably surrounded by darker, Mo- and W-depleted regions. In addition, there are a number of thin bright strips and EDX analyses indicated that they, too, are relatively Mo- and W-rich. In the common grey oxide, the Mo:W:Si composition was the same as that of the (Mo, W)Si_2 phase in the bulk material. XRD results (see Fig. 5) confirmed that this oxide was also composed of MoO_3 and WO_3 or a mixed oxide of (W, Mo)O_3. In order to further investigate the composition of the oxide scale TEM/EDX was used. Parts of the scale were removed and crushed in a mortar. Electron transparent flakes from the oxide scale were then analysed with TEM/EDX. The chemical analysis showed that the scale consisted of small Mo and (Mo, W) containing oxide particles embedded in SiO_2. The (Mo, W) oxide particles typically consist of 10–20 at.% Mo and 5–10 at.% W together with approximately 70 at.% O. At 550 °C MoO_3 can only dissolve 4 mol.% WO_3,[12] which implies that W is not in solid solution in MoO_3. According to the phase diagram[12] a mixed oxide, (W, Mo)O_3, appears to have formed. This shows that the oxide scale is composed of SiO_2, MoO_3, (W, Mo)O_3 and small amounts of WO_3.

As in the O_2 exposure, the composition of such regions in the oxide was constant throughout the scale. However, the appearance of the oxide scale cross-section suggests that, unlike the oxide scale in the O_2 sample, there has been a migration of MoO_3 and WO_3 in this sample oxidised in $O_2 + 10\%H_2O$. The migration might be facilitated in the presence of water vapour due to possible weakening of the Si–O–Si structure by formation of Si–OH bonds.[10] It appears that the MoO_3 and the WoO_3 crystals have congregated to form agglomerates at certain sites, leaving the oxide region in the immediate neighbourhood depleted of Mo and W. These agglomerates take the shape of particles or strips. It is likely that the evaporation of Mo-oxide (and some W-oxide as well) took place from these agglomerates, creating additional voids surrounded by Mo- and W-depleted oxide.

Both oxides scales (O_2 and $O_2 + 10\%H_2O$) at this temperature featured a large number of voids, which resulted in thick but non-protective oxide scale. There is reason to believe that

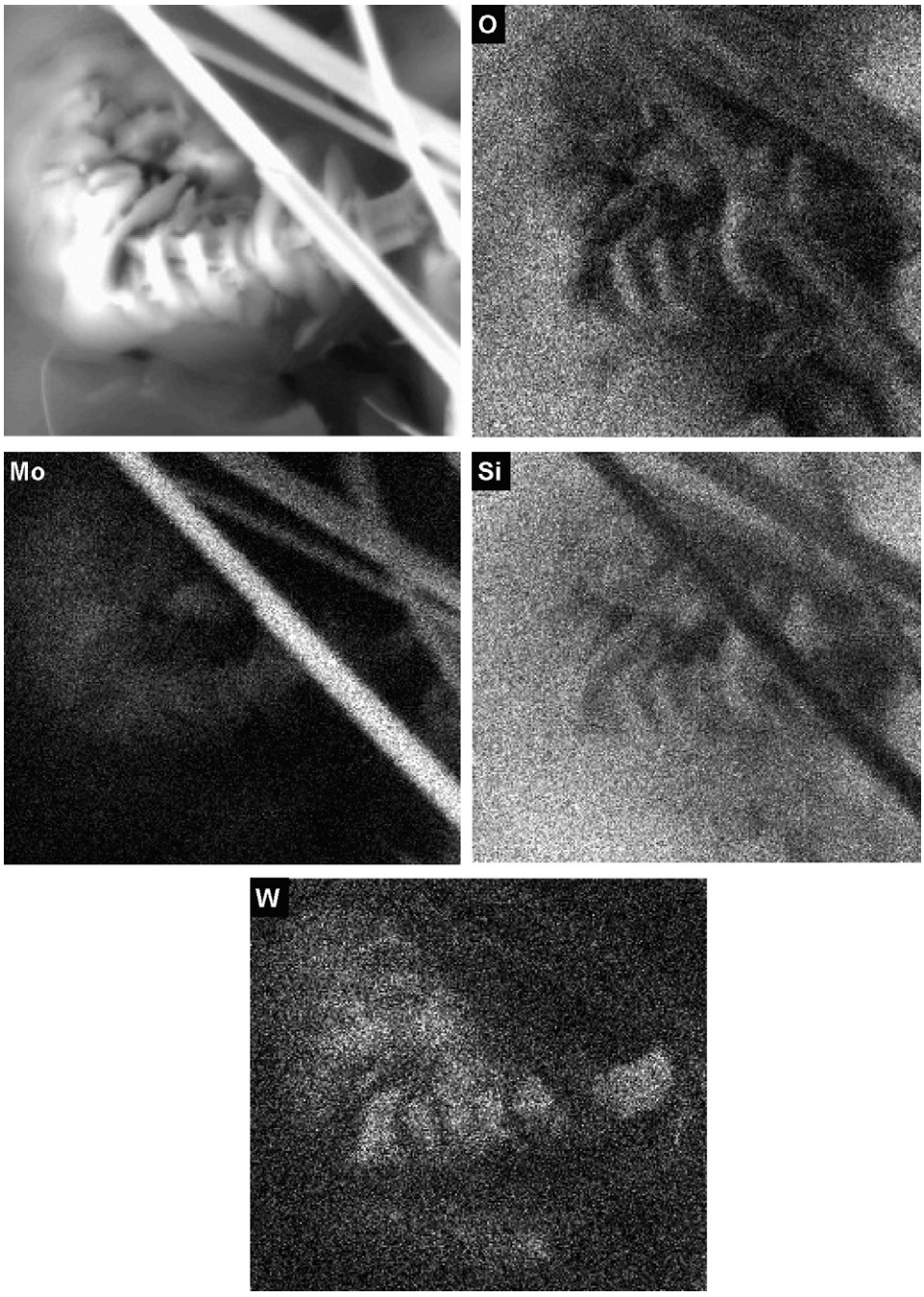

Fig. 15. EDX mapping of the oxide scale formed on a (Mo, W)Si_2 sample exposed at 550 °C in O_2 for 24 h. Light contrast shows the presence of the elements. The needle-shaped oxide consists of Mo and O. The rest of the oxide scale consists of W, Si, Mo and O.

these samples would continue to experience rapid oxide growth in their respective oxidation environments.

3.4.5. Detailed microanalysis on the oxide scale: the 950 °C exposures

Figs. 21 and 11 show SEM backscattered electron images of the oxide scale on the sample oxidised at 950 °C in O_2 for 24 h. As it is past the peak oxidation temperature in O_2, the oxide scale is relatively thin (estimated to be ~10 μm; the oxide scales at 550 °C were at least 3 times thicker). However, the oxide scale is littered with large chunks and smaller particles exhibiting high atomic number contrast. These bright oxide features were found to contain up to 30 at.% W (of cation content) and no more than 5 at.% Mo, with Si accounting for the balance of the cation content. The dark grey regions appear to be mostly SiO_2 with small amounts of W (<6 at.%) but hardly any Mo. It is evident that, at this temperature, the equilibrium vapour pressures of $(MoO_3)n$ species were sufficiently high such that MoO_3 was removed from the oxide scale.

As shown in Figs. 22 and 12, the oxide scale of the sample oxidised in O_2 + 10%H_2O at 950 °C is hardly visible. It appears rather similar to an unoxidised sample. Unlike the O_2 sample,

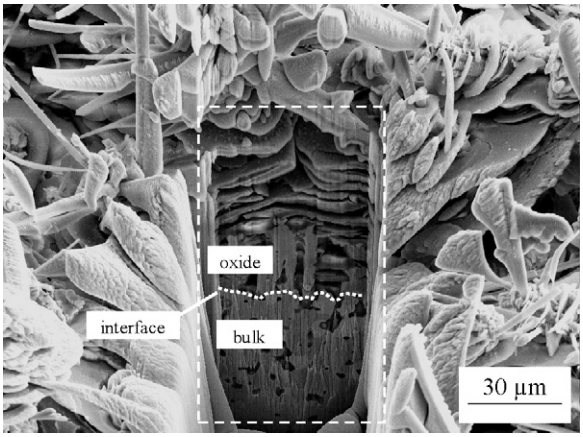

Fig. 16. SEM image of the oxide morphology of a sample oxidised for 24 h at 550 °C in O_2 atmosphere. The cross-section is milled using the FIB and this region is viewed at a 45° tilt angle. The structure is made up of tiers of "petals" and is very open.

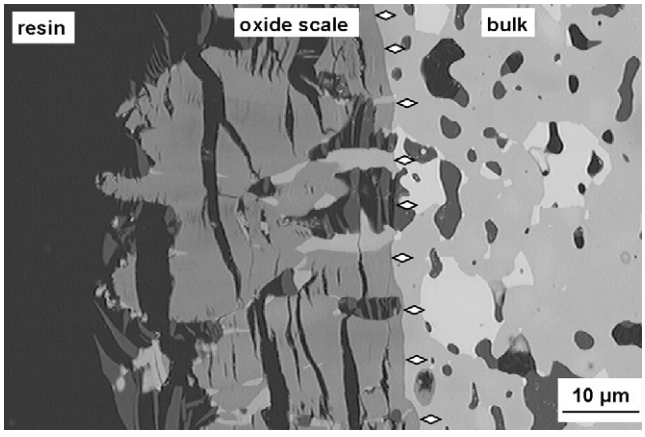

Fig. 17. SEM backscattered electron image of a polished cross-section showing the oxide microstructure of a sample oxidised for 24 h at 550 °C in O_2 atmosphere. The oxide–bulk interface is indicated using diamond-shaped markers.

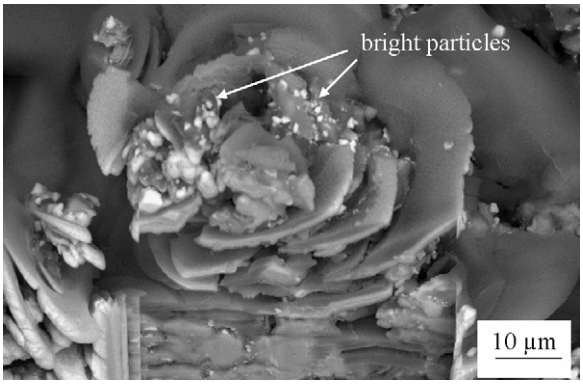

Fig. 18. SEM backscattered electron image of the oxide morphology of a sample oxidised for 24 h at 550 °C in $O_2 + 10\%H_2O$ atmosphere. The rose-like geometry is viewed at a 45° tilt angle. The "petals" of the "rose" contain mostly SiO_2, while the bright particles (indicated) contain mostly Mo- and W-oxide.

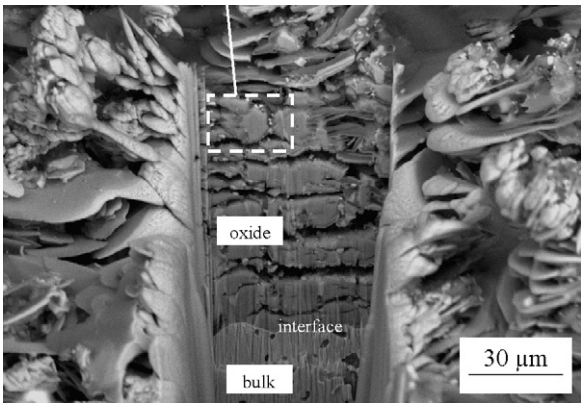

Fig. 19. SEM image of the oxide morphology of a sample oxidised for 24 h at 550 °C in $O_2 + 10\%H_2O$ atmosphere viewed in cross-section at a 45° tilt angle. The structure is characterised by a large number of cracks and voids.

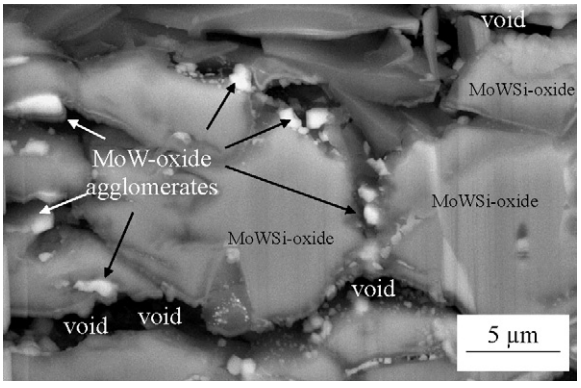

Fig. 20. SEM backscattered electron image of the morphology of the outer oxide (ref. Fig. 16) on a sample oxidised for 24 h at 550 °C in $O_2 + 10\%H_2O$ atmosphere viewed in cross-section at higher magnification at a 45° tilt angle. The general grey region is oxidised (Mo, W)Si_2 (labelled MoWSi-oxide). The white particles appear to be agglomerated Mo- and W-oxides, and are generally surrounded by darker Mo- and W-depleted oxide. They also tend to congregate around voids.

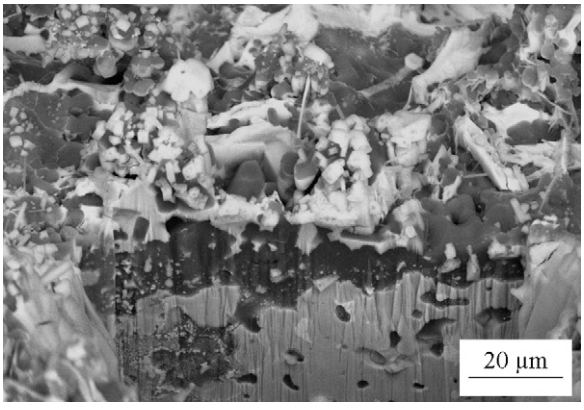

Fig. 21. SEM backscattered electron image of the oxide morphology on a sample oxidised for 24 h at 950 °C in O_2 atmosphere viewed at a 45° tilt angle. The site is milled using the FIB and reveals the cross-section of the oxide scale. The top surface is littered with bright oxide formations that appear to be mostly very W-rich oxide. The dark grey regions are mostly SiO_2.

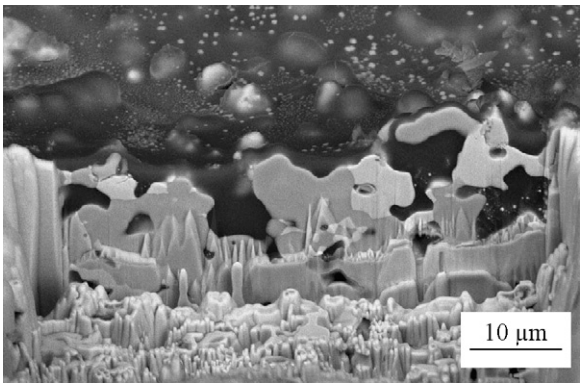

Fig. 22. SEM backscattered electron image of the oxide morphology on a sample oxidised for 24 h at 950 °C in $O_2 + 10\%H_2O$ atmosphere viewed at a 45° tilt angle. The site is milled using the FIB and reveals the cross-section of the oxide scale. The scale is very thin. There are white powder-like particles on the dark grey SiO_2 on the top surface.

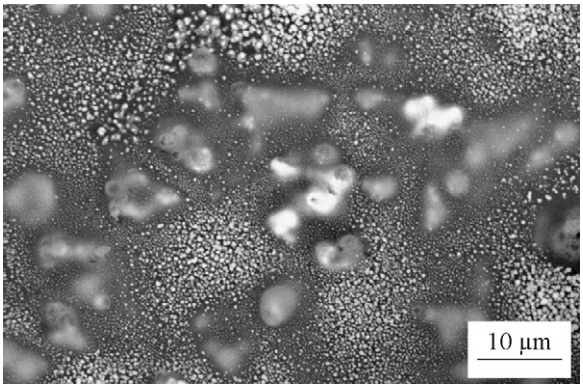

Fig. 23. SEM backscattered electron image of the oxide surface on a sample oxidised for 24 h at 950 °C in $O_2 + 10\%H_2O$ atmosphere viewed from the top. The white powder-like particles on the dark grey SiO_2 are WO_3 that are likely to have been redeposited.

there were no W-rich chunks or particles. However, there were fine powder-like bright particles on the top surface. To verify that it was not an artefact of FIB-milling, the top surface at least 2 mm away from the milled site was investigated (see Fig. 23). The "powder" was present all over the sample surface. EDX analysis indicated that this "powder" was W-rich, which suggests that it might be WO_3. With the presence of water vapour at this temperature, it is likely that the removal of not just MoO_3 but also WO_3 was rather efficient. Thus, owing to the efficient removal of the MoO_3 and WO_3 crystals from oxide scale, and because the healing of SiO_2 voids takes place rapidly enough due to the increased mobility, a dense protective silica could be re-established and maintained. As a result, the oxidation practically ceased after a short period.

4. Conclusion

The investigated (Mo, W)Si_2-based composite was found to exhibit three distinct modes of behaviour in the temperature range 350–950 °C. At 350–450 °C, little oxide is formed because the transport processes at these temperatures are slow. At 550–750 °C, the material undergoes accelerated oxidation, forming large quantities of tungsten and molybdenum oxide particles embedded in silica. The resulting oxide scale is thick but is porous and delicate, offering little if any protection against sustained rapid oxidation. The peak mass gains in dry O_2 and $O_2 + 10\%H_2O$ were found to occur at a temperature of about 750 °C in O_2 and 650 °C in $O_2 + 10\%H_2O$, respectively. The recorded mass gains were significantly larger in O_2 than in $O_2 + 10\%H_2O$. It is believed that this difference is mainly due to the more rapid removal of Mo and W in the form of $MoO_2(OH)_2$ and $WO_2(OH)_2$ species when water vapour is present as the oxide–hydroxides are known to have higher equilibrium vapour pressures than their oxide counterparts. At above 850 °C, the removal of Mo and W from the oxide scales is rapid enough to allow partial healing of the silica, reducing its permeability. It was found that, at 950 °C in $O_2 + 10\%H_2O$, a protective SiO_2 scale could be re-established quickly and maintained, causing the oxidation to practically cease.

Acknowledgements

This work was carried out within the Swedish High Temperature Corrosion Centre (HTC), with financial support partly provided by the Swedish National Research Council (VR).

References

1. Kurokawa, K., Matsuoka, H. and Takahashi, T., High temperature oxidation of $MoSi_2$–WSi_2 solid solutions. *Materials Science Forum*, 1997, **251–254**, 885–892.
2. Kim, H.-S., Yoon, J.-K., Kim, G.-H., Doh, J.-M., Kwun, S.-I. and Hong, K.-T., Growth behaviour and microstructure of oxide scales grown on WSi_2 coating. *Intermetallics*, 2008, **16**, 360–372.
3. Lavrenko, V. A., Shemet, V. Z. and Goncharuk, A. V., Studies on mechanism of high-temperature oxidation of molybdenum, tungsten and zirconium disilicides by differential thermal analysis. *Thermochemica Acta*, 1985, **93**, 501–504.
4. Millner, T. and Neugebauer, J., Volatility of the oxides of tungsten and molybdenum in the presence of water vapour. *Nature*, 1949, **163**, 601–602.
5. Glemser, V. O. and Haeseler, R. V., Uber gasförmige hydroxide des molybdäns und wolframs. *Zeitschrift fur anorganische und allgemeine Chemie*, 1962, Band 316.
6. Berkowitz, J. and Inghram, M. G., Polymeric gaseous species in the sublimation of molybdenum trioxide. *The Journal of Chemical Physics*, 1957, **26**, 842–846.
7. Hansson, K., Svensson, J. E., Halvarsson, M., Tang, J.-E., Sundberg, M. and Pompe, R., Oxidation behaviour of a $MoSi_2$-based composite in different atmospheres in the low temperature range (400–550 °C). *Journal of the European Ceramic Society*, 2004, **24**(13), 3559–3573.
8. Barin, I., *Thermochemical Data of Pure Substances:*. VCH Verlsgsgesellschaft mbh, 1995.
9. *Thermochemical Properties of Inorganic Substances* (*2nd ed.*)., 1991.
10. Shelby, J. E., *Introduction to Glass Science and Technology* (*2nd ed.*)., 2005.
11. Hansson, K., Halvarsson, M., Tang, J. E., Pompe, R., Sundberg, M. and Svensson, J.-E., The beneficial effect of water vapour on the oxidation of a $MoSi_2$ based composite at 600 and 700 °C. *Journal of the European Ceramic Society*, 2005, **25**(1), 1–11.
12. *Gmelin Handbook, W Suppl. Vol. B 6*.